Iranian Society of Acoustics and Vibration

The 13th International Conference on Acoustics and Vibration ISAV2023

20 , 21 Dec 2023 Tehran - Iran

Vibro-Acoustic Behavior of Unbalanced Shaft-Bearing-Pedestal Coupled System with Bearing Faults

Emadaldin Sh Khoram-Nejad[a], Abdolreza Ohadi[b*]

[a] *PhD Candidate, Acoustics Research Laboratory, Mechanical Engineering Department, Amirkabir University of Technology (Tehran Polytechnic), Tehran, Iran.*

[b] *Professor, Acoustics Research Laboratory, Mechanical Engineering Department, Amirkabir University of Technology (Tehran Polytechnic), Tehran, Iran.*

* *Corresponding author e-mail: a_r_ohadi@aut.ac.ir*

Abstract

This paper deals with the effect of faults and shaft unbalances on the rolling element bearings' (REBs) vibro-acoustic behavior. In addition, the vibro-acoustic behavior of the bearing is investigated from the perspective of human visual and auditory senses. First, a dynamic model for an SKF 6205 bearing is considered. This dynamic model includes a shaft, inner ring, outer ring, and bearing pedestal that includes six degrees of freedom (DOF). The nonlinear contact between the bearing balls and the inner/outer rings of the REB is considered using the Hertzian contact theory. To find the displacement and velocity of the inner ring, outer ring, and bearing pedestal, one can solve six nonlinear partial differential equations with the Range-Kutta method. The results show a 4.65% error in the peak-to-peak time response value compared with the reference experimental results, which is a good agreement. The sound pressure level (SPL) in the far field can be calculated assuming the REB three components as cylindrical sound sources. It is very interesting to know the fault detection capability of the human being without using auxiliary tools. By comparing the results, it is shown that sound is a better measure for humans than observing the vibration of the bearing pedestal. Also, without the use of auxiliary tools, humans cannot detect incipient faults either through the sound or vibration of the REBs. It is very clear for humans to identify the shaft eccentricity with both ears and eyes. In addition, in this article, the nonlinear behavior of the dynamic model with increasing fault severity has also been investigated.

Keywords: Rolling element bearing; Bearing fault modeling; Vibro-Acoustic model.

1. Introduction

REBs are a type of bearing whose working is based on the rolling principle. The REBs, which comprise balls or rollers, an inner ring, an outer ring, and a cage, are always susceptible to failure. The reason for the failure, besides the environment and working conditions, is the transfer of significant dynamic forces from the rotating parts of the system to the stationary portion. Another reason for the

REBs' failure is its non-predictable motion of it. Therefore, fault detection and diagnosis of them is of interest to both researchers and industrial technicians.

Fault diagnosis of rotating machinery is one of the most essential issues in various industries. Because every component after a while needs to be repaired and replaced. Studying faults in rotating machines through modeling helps experts understand their behavior better. Bearings are one of the most cru-cial components of rotating machinery systems. Sometimes, only after a certain period of operation of the bearings, they are replaced according to a specific schedule. But this will cause the healthy bearing that could have worked for a longer period to be replaced unnecessarily. Therefore, it is very common that the industrial experts notice the fault in the bearings after hearing the working noise and send reports to replace it as soon as it is possible. The REB structure, component precision, and lubrication status influence the way it performs and the noises it makes. Hence, exploring dynamic and bearing radiation noise modeling presents an intriguing area of investigation for comprehending fault behavior.

Many studies have been performed on the vibration and dynamic behavior of REBs. Most of the papers have investigated the nonlinear dynamic behavior of bearings. Some papers model bearings or rotor-bearing systems as multi-DOF systems [1]–[4] and others model the bearings especially REBs as multi-body systems [5], [6]. Also, certain studies have introduced a technique for generating defective signals from the REBs [7], [8]. In addition, a new bearing system has been introduced by a group of papers to reduce REB vibrations by floating it in oil [9], [10]

However, there are a few studies about sound radiated from a faulty REB. The noise resulting from the working of a faulty REB is usually due to the vibration of the surfaces of its components. For instance, consider an REB with a crack on its inner ring. An impact force is produced as each ball passes the crack location on the inner raceway. Then, the balls, inner race, outer race, cage, and pedestal vibrate because of this fault when the shaft is rotating. Vibratory surfaces make air molecules oscillate, generating sound waves that lead to the generation of radiated noise, which can be heard by the fault diagnosis expert. The literature on bearing research has scanty reports on REBs' acoustic performance. For instance, by examining the SPL of the oil film, which included the rotor imbalance and elastic deformation of the bearing liner, [11], [12] studied the acoustic properties of a hydrodynamic journal bearing. REB noise mechanism and distribution characteristics have not been analyzed. Accordingly, a method to compute noise in high-speed ceramic angular contact ball bearings was proposed by Yan et al. [13]. This method uses both vibration differential equations and multiple sound source features.

In this paper, using a 6-DOF dynamic model, the vibration behavior of a shaft-bearing-pedestal system is investigated. In this model, the three components of REB, the pedestal, inner ring, and outer ring, are considered. To reveal how much noise the REB and its pedestal make, a cylindrical sound model added up the surface velocities in two directions (x and y). Then using multi sound source principle, the total SPL of the REB is calculated.

2. Methodology

In this research, two dynamic and acoustic models were used, which will be explained in the next two sections. The REB model's speed is used to calculate the SPL emitted by its parts in the acoustic model.

2.1 Dynamic model

In this study, a shaft-bearing-pedestal dynamic model is considered as in [14]. The fault called shaft current damage is common in wind power and subway motors, and scholars are interested in how it affects the shaft-bearing-pedestal (SBP) system. The dynamic model of the system with the fault is illustrated in Figure 1.

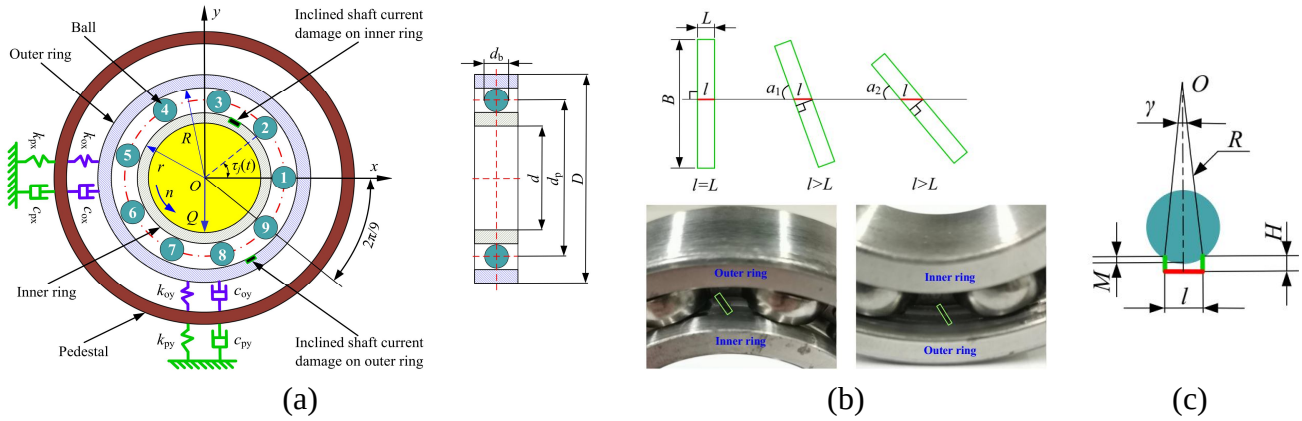

Figure 1: The REB and fault model characteristics; (a) the REB model geometrical parameter, (b) fault geometrical parameters, and (c) parameters related to the behaviour of the balls crossing the fault location [14].

The equations of motion of the REB are as follow:

$$\begin{cases} m_p\ddot{x}_p + c_{px}\dot{x}_p - c_{ox}\left(\dot{x}_o - \dot{x}_p\right) + k_{px}x_p - k_{ox}\left(x_o - x_p\right) = 0, \\ m_p\ddot{y}_p + c_{py}\dot{y}_p - c_{oy}\left(\dot{y}_o - \dot{y}_p\right) + k_{py}y_p - k_{oy}\left(y_o - y_p\right) = 0, \\ m_i\ddot{x}_i + F_{ix} + c_b\left(\dot{x}_i - \dot{x}_o\right) = 0, \\ m_i\ddot{y}_i + F_{iy} + c_b\left(\dot{y}_i - \dot{y}_o\right) = F_{unbalance}, \\ m_o\ddot{x}_o + k_{ox}\left(x_o - x_p\right) - F_{ox} + c_{ox}\left(\dot{x}_o - \dot{x}_p\right) - c_b\left(\dot{x}_i - \dot{x}_o\right) = 0, \\ m_o\ddot{y}_o + k_{oy}\left(y_o - y_p\right) - F_{oy} + c_{oy}\left(\dot{y}_o - \dot{y}_p\right) - c_b\left(\dot{y}_i - \dot{y}_o\right) = 0, \end{cases} \tag{1}$$

where $x_p(t)$, $x_o(t)$, and $x_i(t)$ are the displacement of the pedestal, the outer, and the inner ring on the x-axis, and, $y_p(t)$, $y_o(t)$, and $y_i(t)$ are the displacement of the pedestal, the outer ring and the inner ring on the y-axis. Note that m_p, m_s, and m_o are the mass of the pedestal, the ring and shaft, and the outer ring, respectively. Also, c_{px}, k_{px}, c_{py} and k_{py} are the damping coefficient and stiffness of the pedestal on the x- and y-axis, respectively. In addition, c_{ox}, k_{ox}, c_{oy}, k_{oy}, and c_b are the damping coefficient and stiffness between the outer ring and the pedestal on the x- and y-axis, and the damping coefficient of the ball, respectively.

Using Hertzian contact theory [15], one can expressed the contact forces includes $F_{ix}(t)$, the contact force between the ball and the inner ring on the x-axis, $F_{iy}(t)$, the contact force between the ball and the inner ring on the y-axis, $F_{ox}(t)$, the contact force between the ball and the outer ring on the x-axis, and $F_{oy}(t)$ is the contact force between the ball and the outer ring on the y-axis, as follows:

$$\begin{aligned} F_{ix} &= \sum_{j=1}^{M} k_b \alpha_j^{3/2} H\left(\alpha_j\right)\cos\left(\tau_j\right) \\ F_{iy} &= \sum_{j=1}^{M} k_b \alpha_j^{3/2} H\left(\alpha_j\right)\sin\left(\tau_j\right) \\ F_{ox} &= \sum_{j=1}^{M} k_b \alpha_j^{3/2} H\left(\alpha_j\right)\cos\left(\tau_j\right) \\ F_{oy} &= \sum_{j=1}^{M} k_b \alpha_j^{3/2} H\left(\alpha_j\right)\sin\left(\tau_j\right) \end{aligned} \tag{2}$$

where, M is the number of the balls, k_b is the contact stiffness of the ball, $\alpha_j(t)$ is the total deformation, $H[\alpha_j(t)]$ is Heaviside function, and $\tau_j(t)$ is the position angle of the j-th ball.

The position angle of the *j*-th ball is given by [16]:

$$\tau_j(t) = \omega_p t + 2\pi(j-1)/M, \qquad j = 1, 2, ..., M \tag{3}$$

The total deformation can be calculated as:

$$\alpha_j(t) = [x_i - x_o]\cos(\tau_j) + [y_i - y_o]\sin(\tau_j) - \frac{c_r}{2} - \beta_j \tag{4}$$

where, c_r is the radial clearance, and $\beta_j(t)$ is the additional displacement as shown in Eq. (5).

$$\beta_j(t) = \begin{cases} \left[\frac{d_b}{2} - \sqrt{\frac{d_b^2}{4} - \frac{L^2}{4\cos^2\left(\frac{\pi}{2} - a\right)}}\right]\sin\left(\frac{\pi}{\gamma}\left[\mathrm{mod}(\varphi, 2\pi) - \varepsilon\right]\right); & \varepsilon \le \mathrm{mod}(\varphi, 2\pi) \le \varepsilon + \frac{\gamma}{2} \\ 0; & \textit{else.} \end{cases} \tag{5}$$

Where d_b, L, a, ε, γ, and φ are the ball diameter (Figure 1-a), the length of the fault, the inclination angle, the initial angular offset of fault of the *j*-th ball (Figure 1-b), the damage angle corresponding to the displacement *l*, and the raceway contact angle (Figure 1-c), respectively.

If $\alpha_j(t)$, the contact deformation is positive, the contact force could be calculated using the Hertzian contact theory; otherwise no load is transmitted. It is defined by Heaviside function as [14]:

$$H(\alpha_j) = \begin{cases} 0; & \alpha_j(t) \le 0 \\ 1; & \alpha_j(t) \ge 0 \end{cases} \tag{6}$$

The external force on the inner ring of the y-axis comes from unbalance of the rotor and can be calculated as:

$$F_{unbalance} = -m_i e\omega^2 \sin(\omega t) \tag{7}$$

where *e*, and ω are the eccentricity of the shaft, and rotational speed of shaft.

Solve Eq. (1) with the Runge-Kutta method using ODE 45 in Matlab software results in state vectors which include pedestal, inner, and outer ring velocities. Using these components' velocities, the radiated noise from the REB can be obtained in the next section.

To have an indicator for the displacements of the inner ring, outer ring, and bearing pedestal, one can define the total displacements as:

$$D_j = \sqrt{x_j^2 + y_j^2}, \qquad j = i, o, p$$

2.2 Acoustic model

There are four components to the REBs: the inner ring, the outer ring, the rolling elements (balls or rollers), and the cage and they are placed in a bearing pedestal. The system which study in this paper only considers the dynamics of the inner ring, the outer ring and the pedestal of the bearing. Vibration and shock will cause friction and impact noise in the bearing components during operation. To analyse the noise characteristics of the REB system, the noise produced by each component of the system investigated. The bearing's total radiation noise is the combination of the noise from these three components. There are some assumptions on the medium around the bearing in order to calculate the radiation noise:

- The sound wave propagates through a perfect fluid with no energy loss.
- In the absence of any sound disturbance, the medium is uniform and continuous.
- The medium and its vicinity remain adiabatic during sound wave propagation [13].

In the proposed dynamic model of REB, the DOFs are defined in the radial direction of the REB. REB components in the proposed model move cylindrical during vibration, leading to the use of a cylindrical sound source for measuring radiation noise.

The wave equation for the propagation of the small-amplitude wave in a perfect fluid is [17]:

$$\nabla^2 p - \frac{1}{c^2}\frac{\partial^2 p}{\partial t^2} = 0 \tag{8}$$

Where, *p*, *c*, and *t* are sound pressure, sound velocity in the medium, and the time.
However, for the cylindrical wave sources, it is better to expand Eq. (8) in cylindrical coordinate. Therefore, one can express Eq. (8) as Eq. (9). It is assumed that the *x*-axis coincides with the cylindrical axis. Thus, the sound pressure *p* is independent of the *X* coordinate.

$$\frac{\partial^2 p}{\partial r^2} + \frac{1}{r}\frac{\partial p}{\partial r} = \frac{1}{c^2}\frac{\partial^2 p}{\partial t^2} \tag{9}$$

Where *r* is the distance between observation point and cylinder centre. The far-field and out-of-cylinder solution for Eq. (9) is given by [18]:

$$P(r,\theta,t) = AU.\sqrt{B^2 + C^2}\, e^{j\left(\omega t - kr - \tan^{-1}\frac{C}{B}\right)} \tag{10}$$

Where;

$$A = \frac{\rho_0 c}{\frac{1}{4} + \left(\frac{2}{\pi k^2 a^2}\right)^2}\cos\theta,$$

$$B = \frac{1}{\pi kr} + \frac{r}{\pi k a^2},$$

and

$$C = \frac{kr}{4} + \frac{4}{\pi^2 k^3 r a^2}$$

The surface velocity, *U*, of Eq. (10) is obtained from vibration analysis of the bearing from the previous section.

$$U_j = \sqrt{\dot{x}_j^2 + \dot{y}_j^2}, \qquad j = i, o, p \tag{11}$$

The SPL of a certain sound source is measured by assuming a continuous time interval at a certain fixed position. It is also called the sound pressure RMS-value or the effective sound pressure and can be obtained as follow [11]:

$$p_{RMS} = \sqrt{\frac{1}{T}\int_0^T p^2 dt} \tag{12}$$

where p_{RMS} denotes the RMS of the sound pressure; *p*, the instantaneous sound pressure, and *T*, the sampling time. The effective sound pressure level of *i*-th sound source at the measurement point can be calculated by following expression:

$$L_p^i = 20\log_{10}\frac{p_{RMS}}{p_{ref}} \tag{13}$$

where, $p_{ref} = 2\times10^5$ Pa is the SPL reference value. Eq. (13) calculates the overall SPL of the REB noise at a certain measuring point, based on the principle of sound field superposition [13].

$$SPL = 10\log_{10}\left(\sum_{i=1}^{N} 10^{\frac{L_p^i}{10}}\right) \tag{14}$$

where N is the number of sound sources.

3. Results

In this section, first the correctness of the results obtained is validated in sub-section 3.1. Then, in sub-section 3.2, the vibro-acoustic behavior of REB is investigated.

3.1 Verification results

It is necessary to validate the model of the shaft-bearing-pedestal model results. The model specification is stated in Table 1. For all the results given in this section, the values in Table 1 were used unless it is mentioned in the description. The time responses of the system are shown in Figure 2. The time response of the presented model in Figure 2-a is like the simulation model and experimental system in Figure 2-b and -c from reference [14]. The peak-to-peak values of the presented model and those of the simulation and experimental system are 78.8 m/s^2, 78.8 m/s^2, and 82.63 m/s^2, respectively. The simulation results of [14] and the presented model have a modeling error of 4.63%, which is acceptable compared to the experimental results.

Table 1: The specification of the shaft-bearing-pedestal system.

Parameter [Notation/ unit]	Value	Parameter [Notation/ unit]	Value
Shaft and inner ring mass [m_i/ kg]	4.960	The angle of the defect[/degree]	60
Outer ring mass [m_o/ kg]	0.048	The length of the defect [/mm]	0.975
Pedestal mass [m_p]	8.560	Ball-rings Contact stiffness [k_b/ MN.m$^{-1.5}$]	93.9
Radial clearance [c_r/ μm]	16	Damping coefficient of the ball [c_b/ N.s.m^{-1}]	300
Inner ring radius [r/ mm]	15.547	Pedestal-Outer ring stiffness in x-direction [k_{px}/ MN.m^{-1}]	20.4
Outer ring radius [R/ mm]	23.493	Pedestal-Outer ring stiffness in y-direction [k_{py}/ MN.m^{-1}]	20.4
Ball diameter [d_b/ mm]	7.938	Outer-Inner ring stiffness in x-direction [k_{ox}/ MN.m^{-1}]	13.3
Number of the balls	9	Outer-Inner ring stiffness in y-direction [k_{oy}/ MN.m^{-1}]	11.6
Rotational speed [rpm]	3000	Pedestal-Outer ring damping in x- and y-direction [c_{px}/ N.s.m^{-1}]	200
Eccentricity of the shaft [e/ mm]	0.6	Outer-Inner ring damping in x- and y-direction [c_{ox}/ N.s.m^{-1}]	600

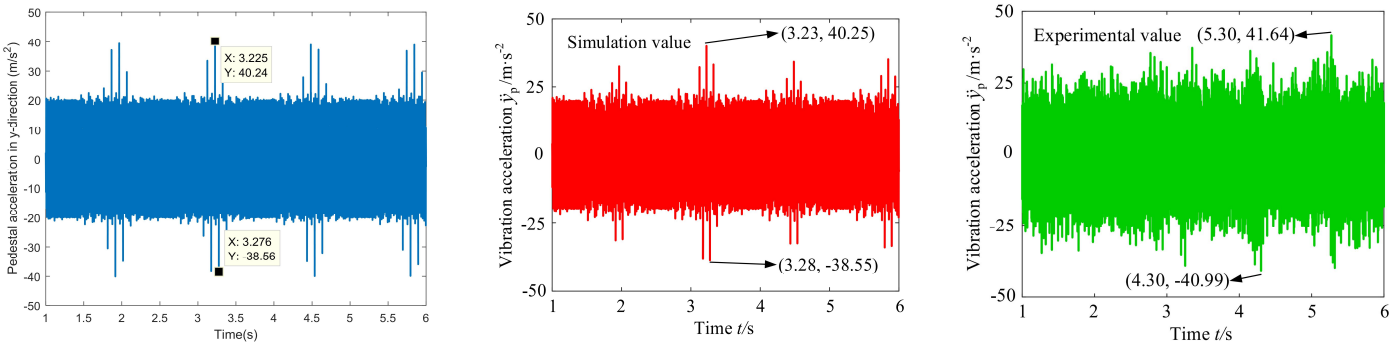

(a) (b) (c)

Figure 2: The comparison between the time responses of (a) the presented model, (b) the simulation model of [14], and (c) the experimental sensors of [14].

3.2 Effect of radial distance of the microphone from the bearing

The effect of microphone location in the radial direction of the REB center on the SPL measured by it is investigated. As it is evident from Figure 3, by moving the microphone away from the REB, the SPL decreases exponentially. The specialized acoustic literature for acoustic sources has experimentally proven this behavior. Notice that the acoustic model presented in this paper is only valid for far field.

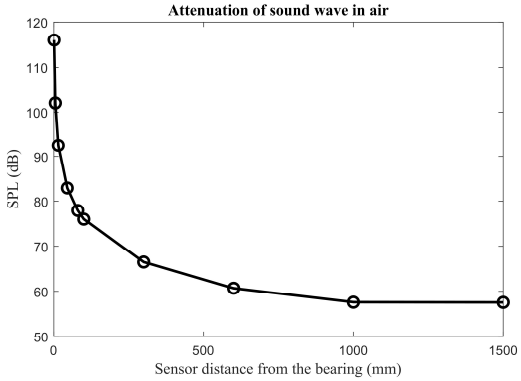

Figure 3: Effect of microphone location in the radius direction of the REB on the SPL emitted from it.

3.3 Effect of fault severity on the vibro-acoustic behaviour of the REB

The experts' comments indicate that it is better to identify the faulty bearing in working condition by listening to its sound than by observing the vibrations of its pedestal, for a rapid decision by human capabilities. In this sub-section, the effect of fault severity (in the means of fault length) on the vibro-acoustic behavior of the REB is investigated in detail. To have a good comparison, the effect of the amount of eccentricity of the shaft on the REB behavior is also investigated. The results are given in this sub-section for inner and outer ring faults separately.
Table 2 shows that the SPL of the healthy REB and the REB with severe fault on the outer ring are different by 2.88 dB. The SPL difference for the REB with severe fault on its inner ring is 2.96 dB (Table 3). In the meantime, the differences between displacement of the pedestal for the healthy and faults on the inner and outer ring are 0.0063 and 0.0068 mm, respectively.

Table 2: Effect of the different outer ring fault severities on the vibro-acoustic behaviour of the REB.

Length of the fault	Without fault	1 mm	3 mm	6.5 mm
SPL (dB)	62.09	62.17	62.89	64.97
D_I (mm)	0.1671	0.1678	0.1702	0.1797
D_O (mm)	0.0406	0.0407	0.0410	0.0450
D_P (mm)	0.0270	0.0272	0.0277	0.0333

Table 3: Effect of the different inner ring fault severities on the vibro-acoustic behaviour of the REB.

Length of the fault	Without fault	1 mm	3 mm	6.5 mm
SPL (dB)	62.09	62.22	63.27	65.05
D_I (mm)	0.1671	0.1685	0.1703	0.1798
D_O (mm)	0.0406	0.0409	0.0413	0.0453
D_P (mm)	0.0270	0.0273	0.0282	0.0338

3.4 Effect of eccentricity on the vibro-acoustic behaviour of REB

The default fault for a majority of rotating machines is the unbalanced fault, which is also taken into account in the presented shaft-bearing-pedestal model. To examine the effect of the eccentricity of the shaft on the SPL and vibration of the REB pedestal, a study was done. The results are reported in Table 4 and the SPL increased from 53.42 dB to 68.15 dB (+ 14.73 dB) as the eccentricity of the shaft increased from 0.1 mm to 1.5 mm.

Table 4: Vibro-acoustic behaviour of the REB with inner ring fault and different shaft eccentricities.

Eccentricity of the shaft	0.1 mm	0.3 mm	0.6 mm	0.9 mm	1.2 mm	1.5 mm
SPL (dB)	53.42	58.49	62.21	67.11	67.61	68.15
D_I (mm)	0.0593	0.1087	0.1686	0.2331	0.2768	0.3211
D_O (mm)	0.0090	0.0222	0.0409	0.0670	0.0818	0.0982
D_P (mm)	0.0061	0.0148	0.0273	0.0470	0.0559	0.0659

3.5 Chaotic behaviour of the system by increasing the fault severity

The nonlinear behaviour of the REBs is also of interest for many researchers and was investigated in this study. A phase plot looks complicated is a sign of chaotic motion. It is possible for motion with a complicated-looking motion to be fully predictable and non-chaotic. The phase plot of a linear system with 1,000 DOF, for instance, may appear complicated, even though it is non-chaotic [19].
In Figure 4 the phase portraits are indicated for different fault severity. Therefore, the complicated-looking motion is due to the growing of the fault. In addition, the inner and outer ring faults are based on nonlinear contact theory and by growing the share of the nonlinear force in the equations, the phase portraits becomes more complicated and it is an indicator for chaotic motion.

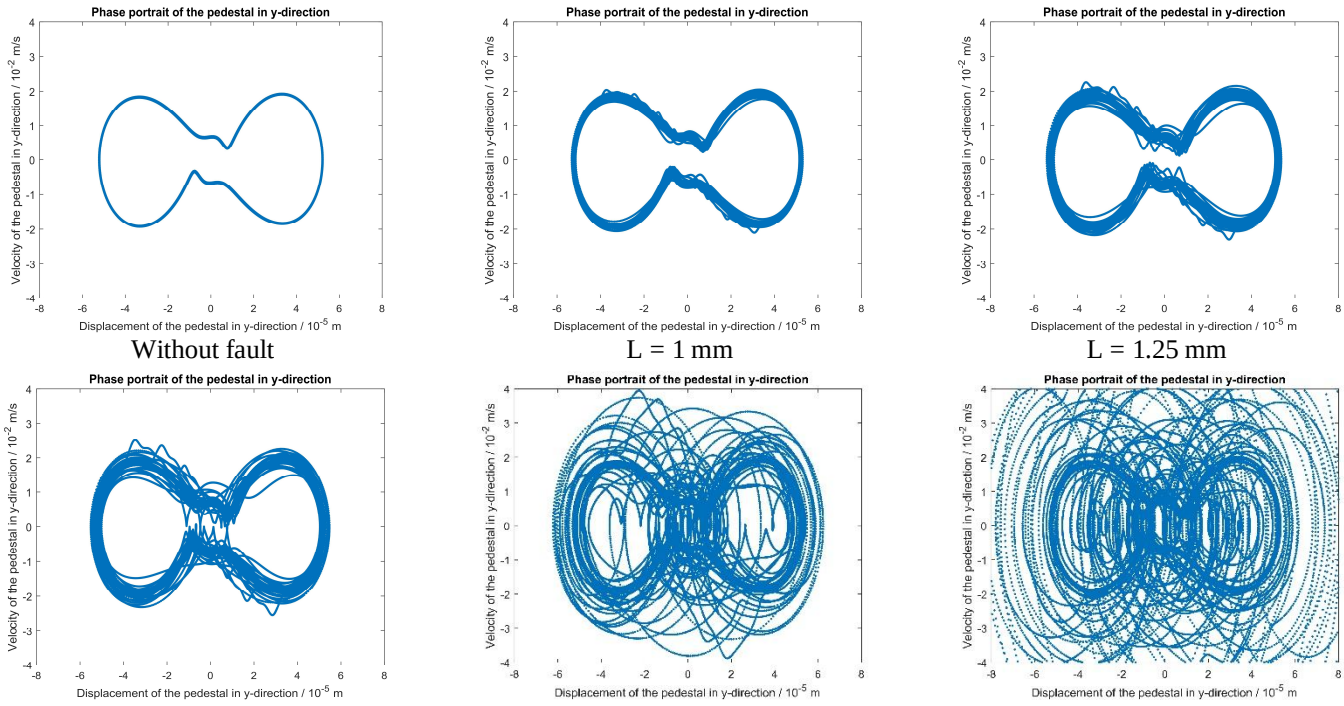

Figure 4: Phase portraits of the pedestal in y-direction for different fault severities.

4. Conclusion

The effect of the bearing faults and unbalanced shaft was investigated on the vibro-acoustic behavior of an SKF 6205 REB. To model the bearing inner and outer ring faults, the nonlinear contact between the bearing balls and the rings was considered using the Hertzian contact theory. The velocity and displacement of the REB model's three components, including the inner ring, outer ring, and bearing pedestal, were obtained by solving the nonlinear partial differential equations. The results showed a small 4.65% error compared with the reference experimental results. By assuming cylindrical sound sources for the three REB model components and having their velocities, the SPL in the far field was computed. It is fascinating to learn how humans can recognize faults with just their eyes or ears. The study concluded that sound is a better measure than vibration for humans. At 6.5 mm fault length, SPL changed by 3 dB, and pedestal displacement changed by 0.0068 mm, which were audible and invisible changes, respectively. For a fault length of 1 mm, compared to the condition without bearing faults, the SPL and bearing pedestal displacement were changed by 0.08 dB and 0.0002 mm, respectively. Therefore, without auxiliary tools, humans cannot detect incipient faults through both sound and vibration. Humans can easily detect shaft eccentricity using their ears and eyes. It is because the SPL was changed by 14.73 dB when eccentricity became 6.5 mm and the pedestal displacement became 0.0659 mm from 0.0061 mm. In addition, in this article, the nonlinear behavior of the dynamic

model with increasing fault severity has also been studied. The more severe the fault, the more complicated the phase portraits and chaotic motion observed. Therefore, it can be concluded that the faults lead to chaotic and non-predictable motion of REBs and the reason for sudden failures in REBs.

REFERENCES

[1] P. Yan, C. Yan, K. Wang, F. Wang, and L. Wu, "5-DOF Dynamic Modeling of Rolling Bearing with Local Defect considering Comprehensive Stiffness under Isothermal Elastohydrodynamic Lubrication," *Shock Vib.*, vol. 2020, pp. 1–15, Jun. 2020, doi: 10.1155/2020/9310278.

[2] X. Cheng, A. Wang, H. Yang, T. Zhang, C. Cao, and G. Wu, "Vibration analysis of a deep groove ball bearing with localized and distributed faults subject to waviness based on an improved model under time-varying speed condition," *J. Vib. Control*, vol. 29, no. 13–14, pp. 3259–3274, Jul. 2023, doi: 10.1177/10775463221094162.

[3] Y. Zhao, Y.-P. Zhu, J. Lin, Q. Han, and Y. Liu, "Analysis of nonlinear vibrations and health assessment of a bearing-rotor with rub-impact based on a data-driven approach," *J. Sound Vib.*, vol. 534, p. 117068, Sep. 2022, doi: 10.1016/j.jsv.2022.117068.

[4] B. Changqing and X. Qingyu, "Dynamic model of ball bearings with internal clearance and waviness," *J. Sound Vib.*, vol. 294, no. 1–2, pp. 23–48, Jun. 2006, doi: 10.1016/j.jsv.2005.10.005.

[5] M. Nakhaeinejad and M. D. Bryant, "Dynamic Modeling of Rolling Element Bearings With Surface Contact Defects Using Bond Graphs," *J. Tribol.*, vol. 133, no. 1, Jan. 2011, doi: 10.1115/1.4003088.

[6] C. Mishra, A. K. Samantaray, and G. Chakraborty, "Bond graph modeling and experimental verification of a novel scheme for fault diagnosis of rolling element bearings in special operating conditions," *J. Sound Vib.*, vol. 377, pp. 302–330, Sep. 2016, doi: 10.1016/j.jsv.2016.05.021.

[7] K. F. Al-Raheem, A. Roy, K. P. Ramachandran, D. K. Harrison, and S. Grainger, "Rolling element bearing faults diagnosis based on autocorrelation of optimized: wavelet de-noising technique," *Int. J. Adv. Manuf. Technol.*, vol. 40, no. 3–4, pp. 393–402, Jan. 2009, doi: 10.1007/s00170-007-1330-3.

[8] D. HO and R. B. RANDALL, "OPTIMISATION OF BEARING DIAGNOSTIC TECHNIQUES USING SIMULATED AND ACTUAL BEARING FAULT SIGNALS," *Mech. Syst. Signal Process.*, vol. 14, no. 5, pp. 763–788, Sep. 2000, doi: 10.1006/mssp.2000.1304.

[9] S. Modaresahmadi, M. Ghazavi, and M. Sheikhzad Saravani, "Dynamic Analysis of a Rotor Supported on Ball Bearings with Waviness and Centralizing Springs and Squeeze Film Dampers," *Int. J. Eng.*, vol. 28, no. 9 (C), 2015, doi: 10.5829/idosi.ije.2015.28.09c.13.

[10] H. Zhou, G. Luo, G. Chen, and F. Wang, "Analysis of the nonlinear dynamic response of a rotor supported on ball bearings with floating-ring squeeze film dampers," *Mech. Mach. Theory*, vol. 59, pp. 65–77, Jan. 2013, doi: 10.1016/j.mechmachtheory.2012.09.002.

[11] B.-H. Rho and K.-W. Kim, "Acoustical properties of hydrodynamic journal bearings," *Tribol. Int.*, vol. 36, no. 1, pp. 61–66, Jan. 2003, doi: 10.1016/S0301-679X(02)00132-9.

[12] S. Bouaziz, T. Fakhfakh, and M. Haddar, "Acoustic Analysis of Hydrodynamic and Elasto-Hydrodynamic Oil Lubricated Journal Bearings," *J. Hydrodyn.*, vol. 24, no. 2, pp. 250–256, Apr. 2012, doi: 10.1016/S1001-6058(11)60241-2.

[13] H. Yan, Y. Wu, J. Sun, H. Wang, and L. Zhang, "Acoustic model of ceramic angular contact ball bearing based on multi-sound source method," *Nonlinear Dyn.*, vol. 99, no. 2, pp. 1155–1177, Jan. 2020, doi: 10.1007/s11071-019-05343-5.

[14] F. Li, X. Li, J. Liu, D. Shang, and H. Ma, "Nonlinear vibration analysis of the shaft-bearing-pedestal coupled system with inclined shaft current damage," *Nonlinear Dyn.*, vol. 111, no. 17, pp. 15853–15872, Sep. 2023, doi: 10.1007/s11071-023-08677-3.

[15] Q. Han and F. Chu, "Nonlinear dynamic model for skidding behavior of angular contact ball bearings," *J. Sound Vib.*, vol. 354, pp. 219–235, Oct. 2015, doi: 10.1016/j.jsv.2015.06.008.

[16] R. Tomovic, V. Miltenovic, M. Banic, and A. Miltenovic, "Vibration response of rigid rotor in unloaded rolling element bearing," *Int. J. Mech. Sci.*, vol. 52, no. 9, pp. 1176–1185, Sep. 2010, doi: 10.1016/j.ijmecsci.2010.05.003.

[17] L. E. Kinsler, A. R. Frey, A. B. Coppens, and J. V Sanders, *Fundamentals of acoustics*. John wiley & sons, 2000.

[18] P. Aslani, S. D. Sommerfeldt, and J. D. Blotter, "Analysis of the external radiation from circular cylindrical shells," *J. Sound Vib.*, vol. 408, pp. 154–167, Nov. 2017, doi: 10.1016/j.jsv.2017.07.021.

[19] J. J. Thomsen, *Vibrations and Stability*. Berlin, Heidelberg: Springer Berlin Heidelberg, 2003. doi: 10.1007/978-3-662-10793-5.